Letter

Interaction-enhanced many-body localization in a generalized Aubry-André model

Ke Huang [1], DinhDuy Vu [2,3], Sankar Das Sarma [2], and Xiao Li [1,*]

[1]*Department of Physics, City University of Hong Kong, Kowloon, Hong Kong SAR, China*

[2]*Condensed Matter Theory Center and Joint Quantum Institute, University of Maryland, College Park, Maryland 20742, USA*

[3]*Department of Physics, Harvard University, Massachusetts 02138, USA*

(Received 4 June 2023; revised 28 December 2023; accepted 16 April 2024; published 7 June 2024)

We study the many-body localization (MBL) transition in a generalized Aubry-André model (also known as the GPD model) introduced by Ganeshan, Pixley, and Das Sarma [Phys. Rev. Lett. **114**, 146601 (2015)]. In contrast to MBL in other disordered or quasiperiodic models, the interaction seems to unexpectedly enhance MBL in the GPD model in some parameter range. To understand this counterintuitive result, we demonstrate that the highest-energy single-particle band in the GPD model is unstable against weak disorder, which leads to this surprising MBL phenomenon in the interacting model. We develop a mean-field theory description to understand the coupling between extended and localized states, which we validate using extensive exact diagonalization and modified density matrix renormalization group (DMRG-X) numerical results.

DOI: 10.1103/PhysRevResearch.6.L022054

Introduction. Interacting many-body systems should manifest the eigenstate thermalization hypothesis (ETH) with long-time thermalization [1–3]. ETH, however, seems to fail generically in one-dimensional (1D) tight-binding models with random or quasiperiodic disorders, at least for finite-size systems, although the situation is unclear in the thermodynamic limit [4–7]. Such a phenomenon is known as many-body localization (MBL) [8–10]. MBL has been numerically and experimentally verified in numerous 1D disordered and quasiperiodic systems with moderate interactions, with the general finding that the disorder strength necessary for inducing MBL is much larger in the interacting system than in the corresponding noninteracting system [8–12]. For example, the noninteracting 1D Anderson model is localized for any finite disorder, whereas the corresponding interacting Anderson model undergoes MBL for large disorder [13]. This is expected as an interaction tends to thermalize the system by sharing energy and information among the constituents, leading to ergodicity as postulated in ETH (all noninteracting systems are trivially nonergodic, whereas the nonergodicity in MBL is nontrivially violating ETH). Another example is the well-known Aubry-André (AA) quasiperiodic model, which has all states localized or extended for a critical "disorder" (i.e., quasiperiodic potential strength) larger or smaller than 1 for the noninteracting model [using the convention in Eq. (2) below], whereas the corresponding interacting model exhibits MBL for disorder larger than 1.7 [11,12,14,15].

Nonetheless, an important question is whether exceptions to the above scenario can be constructed. In the strong interaction regime, an enhanced localization was observed numerically and explained by treating all but the interaction term as perturbation [11,12,16,17]. In this Letter, however, we only focus on the moderate interaction regime, where such a perturbation theory does not apply. To address this question, here we describe and analyze a surprising counterintuitive situation arising in the Ganeshan–Pixley–Das Sarma (GPD) model [18], where finite interactions may lead to enhanced MBL in the sense that MBL occurs "early" with the critical disorder strength for the MBL in the interacting GPD model being lower than that in the noninteracting model. This is unexpected as an interaction is thought to oppose MBL and not induce it. Since the GPD model has already been studied experimentally [19], our predictions are directly verifiable in the laboratory. Note that there have been some earlier works discussing the role of interaction in MBL in specific instances, but our Letter is unique in pointing out the generic role of flat bands and interactions in MBL [20–23]. Our work provides important insights into the competition between localized and extended degrees of freedom in interacting many-body dynamics.

The GPD model. We start with the GPD model, introduced in Ref. [18],

$$H_{\mathrm{GPD}} = \sum_j \left(t c_j^\dagger c_{j+1} + \mathrm{H.c.}\right) + \sum_j V_j n_j, \tag{1}$$

where t is the hopping strength, which is the energy unit in this work. The on-site potential is

$$V_j = \frac{2V\cos(2\pi q j + \phi)}{1 - \alpha\cos(2\pi q j + \phi)}, \tag{2}$$

where $q = (3-\sqrt{5})/2$ (equivalent to the golden ratio), V is the potential strength, $\alpha \in (-1, 1)$, and $\phi \in (0, 2\pi)$ is a

*xiao.li@cityu.edu.hk

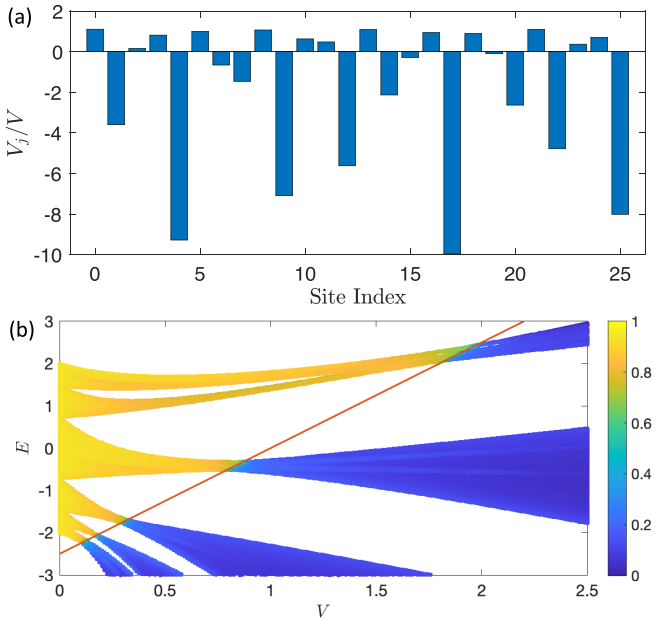

FIG. 1. (a) Quasiperiodic potential of the GPD model in an $L = 26$ system. (b) Fractal dimension of the single-particle GPD model ($U = 0$) in an $L = 610$ system. We take $\phi = 0$, and use the periodic boundary condition to avoid localized edge states. Here (and in all the figures), the α of Eq. (2) is -0.8, and the line defining SPME is given by $E = 5(V - 1)/2$.

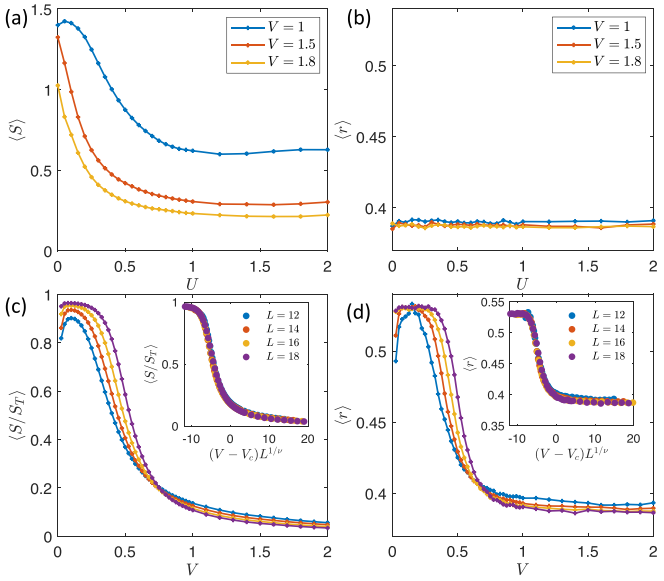

FIG. 2. (a) and (b) show the entanglement entropy and the mean gap ratio averaged over the middle quarter of the spectrum for various V in an $L = 18$ system. (c) and (d) show the same two quantities averaged over the middle quarter of the spectrum for $U = 1$ in systems of various sizes. The insets show the collapse of data as a function of $(V - V_c)L^{1/\nu}$, where $V_c = 0.789$, $\nu = 1.019$ for the EE and $V_c = 0.762$, $\nu = 1.001$ for the mean gap ratio. The result is averaged over 5000, 1000, 200, and 20 random phase realizations for $L = 12$, 14, 16, and 18, respectively.

random phase. The quasiperiodic potential is illustrated in Fig. 1(a).

For $\alpha = 0$, the GPD model reduces to the AA model, which carries no single-particle mobility edge (SPME). However, generic perturbation to the AA model can induce an SPME [12,24–26], and the GPD model with nonzero α is also known to carry an exact SPME given by $\alpha E = 2(1 - V)$ [18]. To show this, we calculate the fractal dimension of the single-particle eigenstates in Fig. 1(b) for $\alpha = -0.8$. The fractal dimension is defined by $\Gamma = -\lim_{L\to\infty} \ln(\sum_j |\psi_j|^4)/\ln L$, where ψ_j is the wave function, and we take $L = 610$ in the numerical calculation of the fractal dimension. Consequently, we have $\Gamma \to 1$ for extended states and $\Gamma \to 0$ for localized states. As shown in Fig. 1(b), the extended and localized states are separated by the exact SPME, and the system is fully localized at $V_{c0} = 2$.

An "early" MBL. We now consider the spinless interacting GPD model at half filling [27–30]. Specifically, the interacting GPD Hamiltonian is given by $H = H_{\rm GPD} + U \sum_j n_j n_{j+1}$, where U is the interaction strength. Throughout this Letter we will take $\phi = 0$, $\alpha = -0.8$, and adopt the open boundary condition, unless specified otherwise. We use two standard diagnostics to obtain the MBL phase diagram in this model: the entanglement entropy (EE) and the mean gap ratio. Here, we use the von Neumann entropy given by $S = -\mathrm{tr}_L[\rho_L \ln \rho_L]$ and $\rho_L = \mathrm{tr}_R|\psi\rangle\langle\psi|$, where $\mathrm{tr}_L, \mathrm{tr}_R$ denote the partial trace over the left and the right half of the system, respectively. In addition, the mean gap ratio $\langle r \rangle$ is defined as the average value of $r_i = \min\{\delta E_i, \delta E_{i+1}\}/\max\{\delta E_i, \delta E_{i+1}\}$, where $\delta E_i = E_{i+1} - E_i$ is the energy gap between two adjacent energies. In the thermal phase, the EE of the eigenstate approaches the Page value $S_T = (L \ln 2 - 1)/2$ [31] and $\langle r \rangle = 0.53$ for the Gaussian orthogonal ensemble. In the MBL phase, we have $S/S_T \to 0$ and $\langle r \rangle = 0.38$ for the Poisson distribution.

In Figs. 2(a) and 2(b), we calculate the EE and the mean gap ratio averaged over the middle quarter of the spectrum for $V = 1.5$. In Figs. 2(c) and 2(d), we obtain the same quantities for $U = 1$. One prominent feature in these results is that the system seems to have an "early" MBL transition as shown in Figs. 2(a) and 2(b). For very weak interactions ($U \ll 1$), the EE is approximately $S_{\rm Slater} = N_{\rm ext}(2 \ln 2 - 1)$, where $N_{\rm ext}$ is the number of the extended single-particle eigenstates [32]. However, as the interaction U increases, the system becomes *localized* rather than thermalized, as shown by the drastic decrease of the EE. Further, we find that the mean gap ratio is always 0.38, suggesting that the system directly enters the MBL phase from the noninteracting limit. To further verify this "early" MBL transition, we take $U = 1$ and analyze the finite-size effect in Figs. 2(c) and 2(d) by collapsing the data as a function of $(V - V_c)L^{1/\nu}$. Both of them indicate an MBL transition around $V_c \approx 0.78$, which is much smaller than the full single-particle localization transition at $V_{c0} = 2$. Furthermore, we find that the critical exponent ν is about 1, in agreement with those studied in the other MBL systems [17,33]. We thus see that the MBL transition in this model happens consistently at a critical disorder strength well below the single-particle localization point. Such a feature is in stark contrast with the MBL transition found in all other models, where MBL happens at a critical

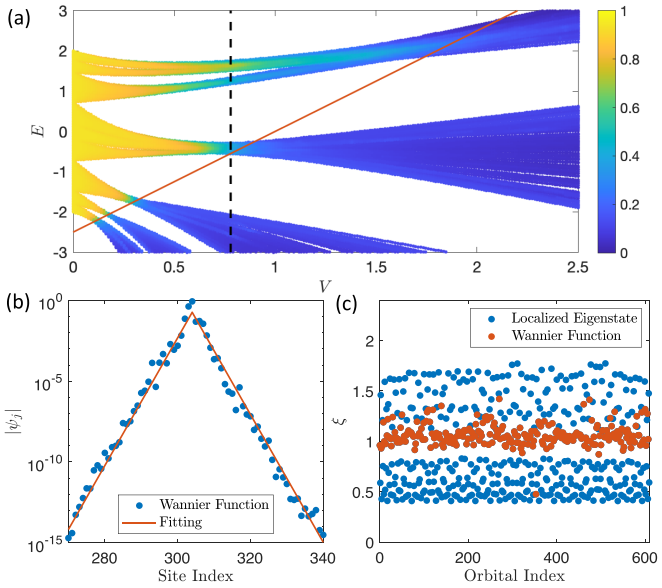

FIG. 3. (a) The fractal dimension of all eigenstates in a single-particle GPD model under the perturbation of Eq. (3). The black dashed line represents the putative MBL transition point $V_c = 0.78$. (b) The wave function of one Wannier function and its fitting. (c) The localization length of the localized eigenstates and the Wannier functions. Here, we take $\phi = 0$ and $L = 610$.

disorder substantially larger than that for the noninteracting case [8–13].

Fragile flat bands. To explain this surprising "early" MBL transition, we take a closer look at the single-particle properties of the GPD model. From Fig. 1, we see that for $V \in (0.85, 2)$, most eigenstates in the model are already localized, and only the highest-energy band remains extended. Moreover, we find numerically that this flat band contains approximately qL states, so nearly 40% of the states are extended for $V \in (0.85, 2)$. Moreover, compared to other bands, the width of this extended band is very small. It turns out that this extended band is very fragile against external perturbations, which distinguishes the GPD model from some other extensively studied models, such as the AA model [32].

We demonstrate this feature by adding to the single-particle GPD model an additional weak random disorder,

$$\delta V = V \sum_j \delta h_j n_j, \tag{3}$$

where δh_j is uniformly distributed in $[-1/10, 1/10]$. We find that, as a result of the above perturbation, the highest-energy band in the GPD model becomes completely localized for $V > 0.85$, as shown in Fig. 3(a). Intuitively, this observation can be understood by noticing that the width of the flat band w is much smaller than the band gap Δ between this flat band and the other states, making this flat band susceptible to perturbations. In particular, as long as the disorder satisfies $w \ll \delta V \ll \Delta$, first-order perturbation theory leads to the following effective Hamiltonian, $H_{\text{eff}} = P\delta V P$, where P is the projection operator of the flat band. Therefore, the system tends to localize the flat-band states in the presence of any disorder, as shown in Fig. 3(b). These localized eigenstates constitute a localized basis of the flat band, so they can be regarded as the Wannier functions for this flat band. Keep in mind, however, that there is no standard definition of a Wannier function in a quasiperiodic system. Consequently, the shape of the Wannier functions is highly dependent on the perturbation we select. Nonetheless, the localization centers of any two Wannier functions are separated by at least two lattice sites, regardless of the choice of perturbation [32]. To quantify the extent of localization, we extract the localization length ξ of the Wannier functions by fitting the wave function to $\psi_j \propto \exp(-|j - j_0|/\xi)$, as shown in Fig. 3(b). Our results in Fig. 3(c) show that all the Wannier functions are deeply localized states with $\xi \sim 1$. Hence, the single-particle GPD model with $\alpha = -0.8$ resembles a deeply localized system disguised by weak tunneling that can be destroyed by the disorder. In fact, the fragile flat band is only prominent for large α (i.e., $|\alpha|$ close to 1) and small q, and therefore our discussion below is strictly carried out in this limit.

A mean-field description of interaction-enhanced MBL. The early MBL transition suggests that the extended orbitals in the flat band, amounting to 40% of all the orbitals, are localized by the other localized single-particle states. Based on our discovery of the fragile flatband in the GPD model, an intuitive argument for the early MBL transition is that quantum fluctuations coming from the localized orbitals serve as the additional disorder and localize the extended flat band as the interaction is turned on. This heuristic viewpoint can be theoretically formulated by a mean-field (MF) theory. The MF theory is essentially a set of nonlinear self-consistent equations, and the physics can be explained by the MF theory if the solution of the self-consistent equations agrees with the numerically calculated many-body eigenstates.

Let us construct a complete and deep-localized basis utilizing the Wannier functions together with the other localized orbitals. Each lattice site can be associated with a unique basis orbital localized on this site. Under this basis, the model of Eq. (1) can be rewritten as

$$H_{\text{GPD}}^{(\text{new})} = \underbrace{\sum_j \epsilon_j \tilde{n}_j + \sum_{i \neq j} U_{ij} \tilde{n}_i \tilde{n}_j}_{\text{dominant}} + \underbrace{\sum_{\substack{i,j \in \text{flat} \\ i \neq j}} t_{ij} f_i^\dagger f_j + {\sum_{ijkl}}' U_{ijkl} f_i^\dagger f_j^\dagger f_k f_l}_{\text{perturbative}}, \tag{4}$$

where f_j annihilates the basis orbital localized on site j, and $\tilde{n}_j = f_j^\dagger f_j$ is the particle number of the orbital j. In addition, $j \in$ flat denotes the Wannier functions of the flat band, and $\sum'_{ijkl}$ denotes that three of the four indices $ijkl$ are different. The first term in Eq. (4) is the energy of the orbital, and the second is the diagonal part of the interaction in this basis, serving as the additional disorder. These two terms contribute the dominant part of the Hamiltonian. The third term comes from the weak tunneling between the Wannier functions, and we estimate that $t_{ij} \sim w/2 \sim O(10^{-1})$. Finally, the last term

is the off-diagonal part of the interaction, and thus

$$U_{ijkl} \sim U \exp[-(\max\{i,j,k,l\} - \min\{i,j,k,l\})/\xi] \lesssim U \exp(-2/\xi) \sim O(10^{-1}). \quad (5)$$

Hence, the last two off-diagonal terms are perturbative, suggesting that the MF theory should work well. Although we choose a specific basis in this argument, the self-consistent equations are basis independent, and so are the MF solutions. Our numerical results below show that the precision of the MF solution is much better than $O(10^{-1})$. The above argument also applies to MBL in other models, and we specifically show for the AA model [32].

Accuracy of the MF solution. We now demonstrate numerically the accuracy of the MF theory. We fix $V = 1.5$, which is smaller than the single-particle localization transition point. The standard MF theory targets low-temperature physics, and thus we need to calculate the ground state of the self-consistent equations $H_{\rm MF}(|\psi\rangle)|\psi\rangle = E|\psi\rangle$, where $|\psi\rangle$ is a Slater determinant, E is the energy, and $H_{\rm MF}(|\psi\rangle)$ is given by

$$\begin{aligned} H_{\rm MF}(|\psi\rangle) = & t\sum_j \left(c_j^\dagger c_{j+1} + \text{H.c.}\right) + \sum_j V_j n_j \\ & + U\sum_j \left(\langle\psi|n_{j-1}|\psi\rangle + \langle\psi|n_{j+1}|\psi\rangle\right) n_j \\ & - U\sum_j \left(\langle\psi|c_j^\dagger c_{j+1}|\psi\rangle c_{j+1}^\dagger c_j + \text{H.c.}\right). \end{aligned} \quad (6)$$

Here, we omit the constant in the MF Hamiltonian. However, to analyze the "early" MBL transition, we must obtain the highly excited solution of the self-consistent equations, which is notoriously difficult in generic models. To derive the highly excited states, we can start from the product state of the localized orbitals, replace the nonlinear terms, and maximize the overlap between the next state and the current state, a procedure resembling the modified density matrix renormalization group (DMRG-X) algorithm [34,35]. If the iteration converges, we then generate an MF state from the initial Fock state. We elaborate on this procedure and provide an improved algorithm in the Supplemental Material [32]. We emphasize that despite the similarity between DMRG-X and our modified MF theory, these two algorithms focus on very different aspects. First, although DMRG-X is expected to provide a more quantitatively accurate approximation, the MF theory provides a more intuitive understanding of the physics behind the numerical results. Second, the MF theory is much faster numerically than the DMRG-X algorithm. Finally, the MF theory can actually provide more accurate initial states for the DMRG-X algorithm.

To illustrate the power of our MF theory, we first study a particular MF solution, the MF Néel state $|Z_2\rangle$ generated by the Néel-like Fock state $f_0^\dagger f_2^\dagger f_4^\dagger \cdots |0\rangle$. In Fig. 4, we compute the fidelity of the MF Néel state $F(t) = |\langle Z_2|Z_2(t)\rangle|$ in an $L = 18$ system using exact diagonalization (ED) and $L = 26$ system using the kernel polynomial method (KPM) [36]. The fidelity in both systems remains surprisingly high (>0.997) and does not decay after 1000 tunneling times. This implies that the MF Néel state is fairly close to one of the many-body eigenstates. To compare the MF Néel state with the

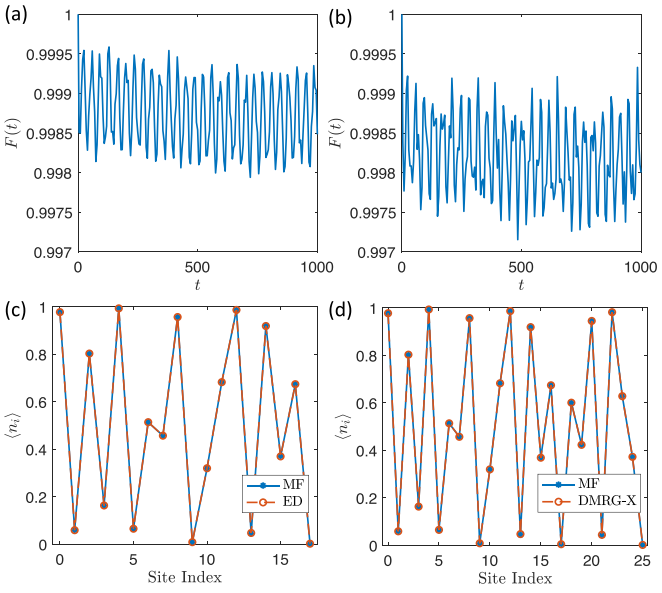

FIG. 4. (a) and (b) show the fidelity $F(t) = |\langle\psi|\psi(t)\rangle|$ of the MF Néel state in an $L = 18$ (using ED) and an $L = 26$ system (using KPM), respectively. (c) and (d) show the expectation of the particle number in the MF Néel states and their corresponding eigenstates derived by ED or DMRG-X. The system size is $L = 18$ in (c) and $L = 26$ in (d). For the DMRG-X algorithm, the energy uncertainty is $\langle H^2\rangle - \langle H\rangle^2 = 2.9 \times 10^{-9}$. Here, we take $\phi = 0$, $V = 1.5$, and $U = 1$.

eigenstates, we use ED to obtain all eigenstates in the $L = 18$ system and choose the eigenstate with the highest overlap (=0.9994) with the MF solution. As shown in Fig. 4, the density profile of the exact eigenstate and that of the MF Néel state are almost indistinguishable. For the $L = 26$ system, we utilize the DMRG-X algorithm with the MF Néel state being the initial state to generate the eigenstate. The DMRG-X algorithm gives us a rather accurate result with the energy uncertainty of $\langle H^2\rangle - \langle H\rangle^2 = 2.9 \times 10^{-9}$. Similar to the result in the smaller system, one can barely differentiate the MF and the DMRG-X results. We also check that the overlap between the DMRG-X and the MF results is $|\langle\psi_{\rm MF}|\psi_{\rm DMRG\text{-}X}\rangle| = 0.9992$. Note that in general, the density profile in the $L = 18$ chain is quite similar to that in the $L = 26$ chain, which shows that the system is deep in the MBL phase. To analyze the finite-size effect, we further validate that the agreement is still excellent up to $L = 68$ [32].

MF theory for generic states. To further validate the MF theory, we now investigate the agreement between generic eigenstates and their corresponding MF solutions. Given that we are focusing on the MBL regime, it is more appropriate to characterize the quality of the approximation using local quantities, such as particle density, rather than global quantities, such as the overlap. Particularly, we plot $f(\delta n)$, the probability density of δn in Fig. 5 with normalization $\int f(\delta)\mathrm{d}\delta n = 1$. This quantity is defined as the absolute value of the particle number difference on a random site between a random eigenstate and its corresponding MF state. To efficiently obtain the corresponding MF solutions of a given eigenstate, we use the one-body reduced density matrix of

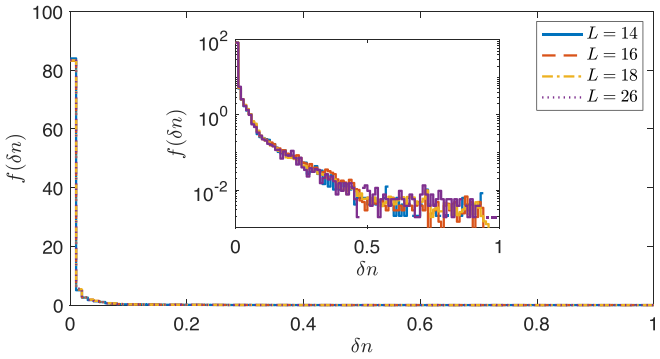

FIG. 5. The probability density $f(\delta n)$ of δn in the GPD model and the inset shows the data in the semilog scale. For $L = 14$, 16, and 18, we consider all the sites and all the eigenstates obtained by ED. For $L = 26$, we consider all the sites and use DMRG-X to generate 2000 random eigenstates. Here, we take $\phi = 0$, $V = 1.5$, and $U = 1$.

the eigenstate $\langle E|c_i^\dagger c_j|E\rangle$ as the initial state for the iteration of the self-consistent equations. We find in Fig. 5 that δn is highly concentrated around zero. What is more, the statistics of the quantity manifest almost no finite-size effects, which can be seen by comparison with the ED results in the smaller systems and the DMRG-X results in the larger system. Hence, the numerical results verify that the MF theory is a general explanation for the "early" MBL transition in the GPD model.

Conclusion. In this Letter, we studied a surprising interaction-enhanced MBL, which is a special feature of the GPD model. This phenomenon is explained by an MF theory construction, which is validated by comparison with numerical results obtained by ED and DMRG-X algorithms. Given the recent experimental implementation of the GPD model [19], our predictions can be experimentally verified.

Acknowledgments. This work is supported by the Laboratory for Physical Sciences, the Research Grants Council of Hong Kong (Grants No. CityU 21304720, No. CityU 11300421, No. CityU 11304823, and No. C7012-21G), and City University of Hong Kong (Project No. 9610428). K.H. is also supported by the Hong Kong Ph.D. Fellowship Scheme.

[1] J. M. Deutsch, Quantum statistical mechanics in a closed system, Phys. Rev. A **43**, 2046 (1991).
[2] M. Srednicki, Chaos and quantum thermalization, Phys. Rev. E **50**, 888 (1994).
[3] M. Rigol, V. Dunjko, and M. Olshanii, Thermalization and its mechanism for generic isolated quantum systems, Nature (London) **452**, 854 (2008).
[4] J. Šuntajs, J. Bonča, T. Prosen, and L. Vidmar, Quantum chaos challenges many-body localization, Phys. Rev. E **102**, 062144 (2020).
[5] A. Morningstar, L. Colmenarez, V. Khemani, D. J. Luitz, and D. A. Huse, Avalanches and many-body resonances in many-body localized systems, Phys. Rev. B **105**, 174205 (2022).
[6] D. Sels, Bath-induced delocalization in interacting disordered spin chains, Phys. Rev. B **106**, L020202 (2022).
[7] H. Ha, A. Morningstar, and D. A. Huse, Many-body resonances in the avalanche instability of many-body localization, Phys. Rev. Lett. **130**, 250405 (2023).
[8] R. Nandkishore and D. A. Huse, Many-body localization and thermalization in quantum statistical mechanics, Annu. Rev. Condens. Matter Phys. **6**, 15 (2015).
[9] E. Altman and R. Vosk, Universal dynamics and renormalization in many-body-localized systems, Annu. Rev. Condens. Matter Phys. **6**, 383 (2015).
[10] D. A. Abanin, E. Altman, I. Bloch, and M. Serbyn, *Colloquium:* Many-body localization, thermalization, and entanglement, Rev. Mod. Phys. **91**, 021001 (2019).
[11] D. D. Vu, K. Huang, X. Li, and S. Das Sarma, Fermionic many-body localization for random and quasiperiodic systems in the presence of short- and long-range interactions, Phys. Rev. Lett. **128**, 146601 (2022).
[12] K. Huang, D. D. Vu, X. Li, and S. Das Sarma, Incommensurate many-body localization in the presence of long-range hopping and single-particle mobility edge, Phys. Rev. B **107**, 035129 (2023).
[13] J. Z. Imbrie, On many-body localization for quantum spin chains, J. Stat. Phys. **163**, 998 (2016).
[14] M. Schreiber, S. S. Hodgman, P. Bordia, H. P. Lüschen, M. H. Fischer, R. Vosk, E. Altman, U. Schneider, and I. Bloch, Observation of many-body localization of interacting fermions in a quasirandom optical lattice, Science **349**, 842 (2015).
[15] T. Kohlert, S. Scherg, X. Li, H. P. Lüschen, S. Das Sarma, I. Bloch, and M. Aidelsburger, Observation of many-body localization in a one-dimensional system with a single-particle mobility edge, Phys. Rev. Lett. **122**, 170403 (2019).
[16] Y. Bar Lev, G. Cohen, and D. R. Reichman, Absence of diffusion in an interacting system of spinless fermions on a one-dimensional disordered lattice, Phys. Rev. Lett. **114**, 100601 (2015).
[17] G. De Tomasi, D. Hetterich, P. Sala, and F. Pollmann, Dynamics of strongly interacting systems: From Fock-space fragmentation to many-body localization, Phys. Rev. B **100**, 214313 (2019).
[18] S. Ganeshan, J. H. Pixley, and S. Das Sarma, Nearest neighbor tight binding models with an exact mobility edge in one dimension, Phys. Rev. Lett. **114**, 146601 (2015).
[19] F. A. An, K. Padavić, E. J. Meier, S. Hegde, S. Ganeshan, J. H. Pixley, S. Vishveshwara, and B. Gadway, Interactions and mobility edges: Observing the generalized Aubry-André model, Phys. Rev. Lett. **126**, 040603 (2021).
[20] X. Li, D.-L. Deng, Y.-L. Wu, and S. Das Sarma, Statistical bubble localization with random interactions, Phys. Rev. B **95**, 020201(R) (2017).
[21] A. P. Vieira and J. A. Hoyos, Emergent dimerization and localization in disordered quantum chains, Phys. Rev. B **98**, 104203 (2018).
[22] N. Macé, N. Laflorencie, and F. Alet, Many-body localization in a quasiperiodic Fibonacci chain, SciPost Phys. **6**, 50 (2019).
[23] A. Štrkalj, E. V. H. Doggen, I. V. Gornyi, and O. Zilberberg, Many-body localization in the interpolating Aubry-André-Fibonacci model, Phys. Rev. Res. **3**, 033257 (2021).

[24] R. B. Diener, G. A. Georgakis, J. Zhong, M. Raizen, and Q. Niu, Transition between extended and localized states in a one-dimensional incommensurate optical lattice, Phys. Rev. A **64**, 033416 (2001).

[25] D. J. Boers, B. Goedeke, D. Hinrichs, and M. Holthaus, Mobility edges in bichromatic optical lattices, Phys. Rev. A **75**, 063404 (2007).

[26] X. Li, X.-P. Li, and S. Das Sarma, Mobility edges in one-dimensional bichromatic incommensurate potentials, Phys. Rev. B **96**, 085119 (2017).

[27] X. Li, S. Ganeshan, J. H. Pixley, and S. Das Sarma, Many-body localization and quantum nonergodicity in a model with a single-particle mobility edge, Phys. Rev. Lett. **115**, 186601 (2015).

[28] X. Li, J. H. Pixley, D.-L. Deng, S. Ganeshan, and S. Das Sarma, Quantum nonergodicity and fermion localization in a system with a single-particle mobility edge, Phys. Rev. B **93**, 184204 (2016).

[29] D.-L. Deng, S. Ganeshan, X.-P. Li, R. Modak, S. Mukerjee, and J. Pixley, Many-body localization in incommensurate models with a mobility edge, Ann. Phys. **529**, 1600399 (2017).

[30] Y.-T. Hsu, X. Li, D.-L. Deng, and S. Das Sarma, Machine learning many-body localization: Search for the elusive nonergodic metal, Phys. Rev. Lett. **121**, 245701 (2018).

[31] D. N. Page, Average entropy of a subsystem, Phys. Rev. Lett. **71**, 1291 (1993).

[32] See Supplemental Material at http://link.aps.org/supplemental/10.1103/PhysRevResearch.6.L022054 for additional data for the stability of other quasiperiodic models under disorder, and also the application of MF theory in the interacting AA model.

[33] V. Khemani, D. N. Sheng, and D. A. Huse, Two universality classes for the many-body localization transition, Phys. Rev. Lett. **119**, 075702 (2017).

[34] V. Khemani, F. Pollmann, and S. L. Sondhi, Obtaining highly excited eigenstates of many-body localized Hamiltonians by the density matrix renormalization group approach, Phys. Rev. Lett. **116**, 247204 (2016).

[35] T. Devakul, V. Khemani, F. Pollmann, D. A. Huse, and S. L. Sondhi, Obtaining highly excited eigenstates of the localized XX chain via DMRG-X, Philos. Trans. R. Soc. A **375**, 20160431 (2017).

[36] A. Weiße, G. Wellein, A. Alvermann, and H. Fehske, The kernel polynomial method, Rev. Mod. Phys. **78**, 275 (2006).